

# Iterative Causal Discovery: Per-Edge Impossibility Certificates, Tier-Aware Oracle Queries, and the $1+K$ Lower Bound

Eichi Uehara  
aflo, Inc., Tokyo, Japan  
eichi.uehara@aflo.one

May 28, 2026

## Abstract

Causal-discovery algorithms return a directed graph, yet provide no principled means of distinguishing edge directions identified by the data from those assigned without an identifying assumption. Under the standard Markov and faithfulness conditions, the observational distribution identifies only a Markov equivalence class; orientations within that class are not determined by the joint distribution and cannot be recovered from additional samples alone, but require either a functional restriction or an intervention. We introduce a protocol for observational causal discovery on continuous data that attaches to each candidate edge a discrete *impossibility certificate*: a `RESOLVED_*` code records the identifiability theorem under which the direction was committed, while an `IMPOSSIBLE_*` code records the failure mode together with the specific question a domain expert must answer to resolve it. The bivariate cascade is extended with five gated identifiability tiers—LSNM, IGCI, Stein, MDL, and PEIT—that abstain when their precondition test rejects. Two oracle primitives, the meta-hub query and the node-children query, jointly establish an upper bound of  $1+K$  expert interactions sufficient to recover any DAG, where  $K$  denotes the number of non-leaf vertices. Under an ideal-oracle assumption, the bound is met exactly on the *asia*, *sachs*, *child*, and *alarm* benchmarks.

## 1 Introduction

Causal structure underpins counterfactual reasoning, intervention design, and out-of-distribution generalisation (Pearl, 2009; Schölkopf et al., 2021; Peters et al., 2017), and its recovery from observational data is a long-standing objective of machine learning. Existing algorithms scale to graphs of hundreds of vertices and return a directed graph estimate, but do not indicate, for each edge, whether the assigned orientation was identified by the data or imposed by the algorithm in order to satisfy its output format. The distinction is material: several widely used continuous-optimisation methods have been shown to exploit data-generation artefacts such as varsortability (Reisach et al., 2021; Kaiser and Sipos, 2022), and without a per-edge record of identification such artefacts are indistinguishable from genuine identification.

The underlying identifiability obstacle is classical. Under the standard Markov and faithfulness conditions, the observational distribution identifies only a Markov equivalence class: orientations of edges that do not lie on a *v*-structure are not determined by the joint distribution, and no algorithm operating on that distribution alone can recover them (Glymour et al., 2019; Pearl, 2009; Spirtes et al., 2000). Breaking the equivalence class requires either an additional functional restriction—an additive-noise model (Hoyer et al., 2008), LiNGAM (Shimizu et al., 2006, 2011), location-scale noise (Strobl and Lasko, 2023; Immer et al., 2023), the information-geometric assumption of IGCI (Janzing et al., 2012), Stein-score identifiability (Rolland et al., 2022), or the algorithmic Markov condition (Janzing and Schölkopf, 2010)—or an intervention (Eberhardt et al., 2005; Hauser and Bühlmann, 2014; Tigas et al., 2022); increasing the sample size does not.

Mooij et al. (2016) survey the bivariate identifiability landscape and document the substantial fraction of empirical edges that fall outside any single one of these regimes.

The present analysis is restricted to observational data with *continuous* variables, for which the residualisation that underlies the cascade tiers and the multi-tier mediator search is well-defined. Extension of the certification pipeline to discrete Bayesian networks constitutes a separate line of future work; the discrete-BN runs reported in Section 4 exercise only the oracle layer and serve as a robustness check, not as the intended deployment regime.

Within this scope, a faithful causal-discovery method may, for any candidate edge  $(X, Y)$ , return one of three responses: (i) the data identifies a direction under a named theorem; (ii) the apparent dependence is mediated by an observed variable, so that the edge is not direct; or (iii) the data are insufficient, and a specific prior question would resolve the orientation. The literature provides theoretical foundations for (i) (Hoyer et al., 2008; Shimizu et al., 2006; Zhang and Hyvärinen, 2009; Janzing et al., 2012; Strobl and Lasko, 2023; Rolland et al., 2022; Hyvärinen and Smith, 2013), classical machinery for (ii) (Spirtes et al., 2000; Colombo et al., 2012), and three established regimes for (iii): linear-Gaussian pairs (Pearl, 2009), latent confounding, and finite-sample regressor misspecification (Mooij et al., 2016). Existing methods pursue distinct design goals (Figure 1) and consequently fail to separate these three responses at the edge level. Continuous-optimisation frameworks (NOTEARS (Zheng et al., 2018), DAGMA (Bello et al., 2022), DirectLiNGAM (Shimizu et al., 2011), and the score-based PC and GES methods (Kalisch and Bühlmann, 2007; Chickering, 2002)) scale to large graphs by returning a fully oriented DAG; in doing so, type-(iii) edges receive a direction selected by the optimisation objective rather than by the data. Constraint-based methods (FCI (Spirtes et al., 2000; Zhang, 2008) and its PAG output) correctly leave type-(iii) edges undirected, but do not specify the prior input that would resolve each. Bayesian DAG-posterior methods (DiBS (Lorch et al., 2021), BCD-Nets (Cundy et al., 2021), AVICI (Lorch et al., 2022), VCN (Annadani et al., 2021)) return per-edge marginal probabilities, which can be viewed as a soft analogue of an identifiability statement; the probabilities marginalise over assumptions rather than identifying which assumption resolves a given edge. Active-learning methods (He and Geng, 2008; Shanmugam et al., 2015; Hauser and Bühlmann, 2014; Tigas et al., 2022) elicit interventions or topological orders, typically at a budget exceeding what type-(iii) edges alone require. The protocol proposed below addresses this gap by isolating the type-(iii) edges and identifying, for each, the question whose answer would resolve it.

The protocol emits, for each candidate edge of a data-only skeleton, one label drawn from a fixed discrete code set (Figure 2). Two `RESOLVED_*` codes correspond to response (i)—the data identifies a direction under a named theorem—and (ii)—the edge is mediated. A family of `IMPOSSIBLE_*` codes corresponds to response (iii); each code records the specific failure mode (linear-Gaussian, latent-likely, regressor-inconsistent, four regime-specific codes for circular, binary-continuous, count, and high-cardinality data, and one cross-tier-disagreement code) together with the question a domain expert would be required to answer. The bivariate cascade is extended with five new identifiability tiers (LSNM (Strobl and Lasko, 2023; Immer et al., 2023), IGCI (Janzing et al., 2012), Stein (Rolland et al., 2022), MDL (Janzing and Schölkopf, 2010), and PEIT); each tier is preconditioned by a statistical test, and a tier whose precondition is rejected *abstains*, demoting the candidate to an `IMPOSSIBLE_*` label rather than issuing an orientation the tier cannot certify. Two oracle primitives, the *meta-hub query*—a single interaction returning the top- $K$  network hubs—and the *node-children query*—a single interaction returning a node’s direct children—permit a hub-aware practitioner to commit every outgoing edge of a node in a single query.

Relative to the methods reviewed in Section 2, the proposed protocol provides four guarantees:

1. **Per-edge auditability.** Every committed orientation records the theorem under which it was issued ( $L_0$ ,  $L_1$ ,  $L_{\text{LSNM}}$ ,  $L_{\text{IGCI}}$ ,  $L_{\text{Stein}}$ ,  $L_{\text{MDL}}$ ,  $L_2$ ,  $L_{\text{PEIT}}$ , mediator search, or oracle); every uncommitted edge records the corresponding failure mode.

<b>Forced-DAG</b> PC, GES, NOTEARS DAGMA, Di rectLiNGAM	Commit a direction on every edge for scalability $\Rightarrow$ unidentifiable edges receive a forced direction without a per-edge diagnostic of whether data or the optimiser chose it.
<b>PAG / FCI</b>	Mark ambiguous edges undirected $\Rightarrow$ correct, but no targeted question per edge for the practitioner.
<b>Full-tier / active-learning</b>	Ask for a full topological order or interventions ( $V \log_2 V$ bits up front) $\Rightarrow$ over-asks on the easy edges, still under-resolves the hard ones.
<b>This paper: per-edge certificates</b>	RESOLVED_*: data identifies direction under a named theorem, or edge is mediated. IMPOSSIBLE_*: data insufficient $\Rightarrow$ certificate names the specific question to ask.

Figure 1: Existing causal-discovery output formats and the per-edge certificate alternative. Forced-DAG and PAG methods target different design goals (scalability and sound non-identifiability marking, respectively); the proposed protocol addresses an orthogonal goal by identifying, for each unidentifiable edge, the question whose answer would resolve it.

- 2. Abstention in place of forced orientation on unidentifiable edges.** Each cascade tier abstains when its precondition is rejected, and the cross-tier disagreement guard demotes any commit that a higher-precision tier contradicts; a candidate that would otherwise be force-oriented is relabelled IMPOSSIBLE\_\*.
- 3. Targeted prior elicitation.** Only IMPOSSIBLE edges are presented to the practitioner, each accompanied by the question that resolves its failure mode. Two interaction types are supported: a per-edge query returning one of FWD / BWD / ABSENT, and a node-children query that commits all outgoing edges of a node in a single interaction.
- 4. Information-theoretic floor of  $1+K$  interactions under an ideal-oracle assumption.** Provided a domain expert answers each meta-hub and node-children query correctly, the protocol recovers the ground-truth DAG at precision = recall = 1.000 in exactly  $1+K$  interactions, where  $K$  denotes the number of non-leaf vertices (Theorem 1). The bound is information-theoretic and holds independently of the edge count; performance under noisy or probabilistic elicitation is deferred to future work.

These guarantees are verified on standard benchmarks (asia, sachs, child, and alarm; Figure 3) and on synthetic data designed to isolate each new tier (Section 4). The protocol is deterministic given a seed; the largest benchmark (alarm,  $V=37$ ) was reproduced end-to-end on a remote Ray cluster.

## 2 Related work

The related literature is organised below into five strands, each addressing one component of the problem considered in this paper.

Continuous-optimisation methods cast structure learning as a differentiable problem and return a fully oriented DAG. NOTEARS (Zheng et al., 2018), DAGMA (Bello et al., 2022), and DirectLiNGAM (Shimizu et al., 2011) are representative; the forced-commitment design favours scalability but does not expose, per edge, whether the chosen direction was identified by the data or assigned by the optimiser.

Constraint-based methods are the historical alternative and rely on conditional-independence testing. PC (Kalisch and Bühlmann, 2007), GES (Chickering, 2002), and FCI (Spirtes et al., 2000; Zhang, 2008) return a CPDAG or PAG, leaving unidentifiable edges undirected. They are sound on the unidentifiable set, yet do not name the specific prior input that would resolve each undirected edge.

A third line treats the DAG as a random variable and learns a posterior over structures.

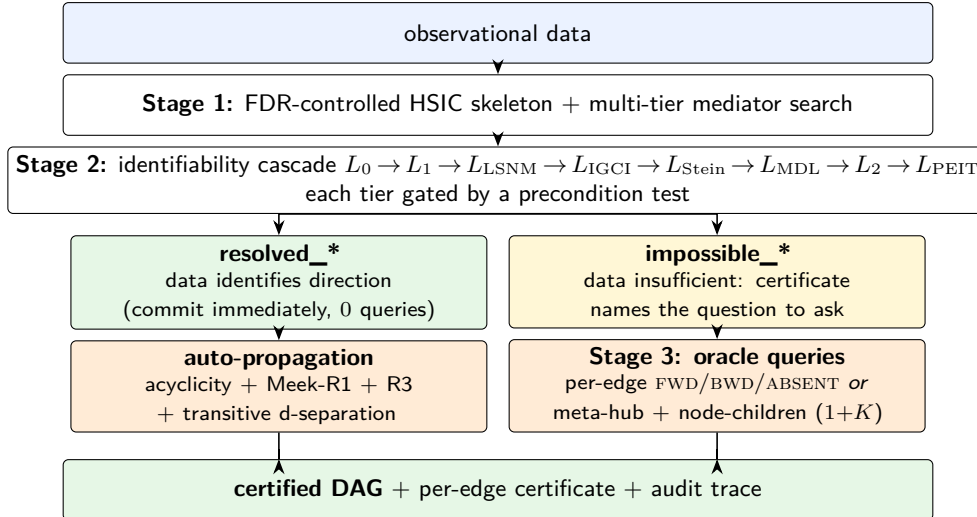


Figure 2: Protocol overview. Stage 2’s cascade contains five new gated safe tiers (LSNM, IGCI, Stein, MDL, PEIT) in addition to the classical  $L_0/L_1/L_2$  ANM lattice. Each tier abstains when its precondition test fails, so a candidate that would otherwise be committed under an incorrect assumption is relabelled IMPOSSIBLE\_\*. Stage 3 issues either per-edge queries or meta-hub + node-children queries.

DiBS (Lorch et al., 2021), BCD-Nets (Cundy et al., 2021), AVICI (Lorch et al., 2022), and VCN (Annadani et al., 2021) return per-edge marginal posterior probabilities, which can be read as a soft analogue of an impossibility certificate. Our protocol differs by emitting a discrete, theorem-tagged code per edge that names the failure mode and the practitioner question, rather than a probability that marginalises over assumptions.

A parallel literature bounds the number of *interventions* required to identify a DAG. Eberhardt et al. (2005), Hauser and Bühlmann (2014), and Tigas et al. (2022); Shanmugam et al. (2015); He and Geng (2008) provide such budgets; the node-children query proposed in this paper is a non-interventional analogue, in which the practitioner enumerates the direct children of a node rather than performing an intervention upon it. The  $1+K$  count established in Section 4 is the elicitation-side counterpart of those intervention budgets.

The use of expert input to refine causal structure has a long history. Heckerman et al. (1995) pioneered prior elicitation for Bayesian-network learning, and Russo and Toni (2023) introduce an argumentation framework for interactive causal discovery. The present work extends this line by combining the bivariate identifiability cascade with the per-edge certificate, so that elicited prior input is requested only at the edges that require it, and only through the question that resolves the certificate code.

### 3 Methodology

Given an observational dataset  $X \in \mathbb{R}^{N \times V}$ , the protocol emits, for every candidate edge in a data-only skeleton, one label drawn from a fixed code set: RESOLVED\_\* when the data identifies the direction (or the edge is mediated), and IMPOSSIBLE\_\* when the data is insufficient, in which case the label names the question the practitioner must answer. The protocol comprises three stages: (1) skeleton construction and multi-tier mediator search; (2) an eight-tier identifiability cascade with precondition-gated commits; and (3) targeted oracle queries on the IMPOSSIBLE residual, interleaved with auto-propagation after each commit. The protocol is deterministic given a seed. The cascade-then-oracle composition is presented below as a query-minimisation algorithm, followed by a description of the data-only stage and of the oracle interaction layer.

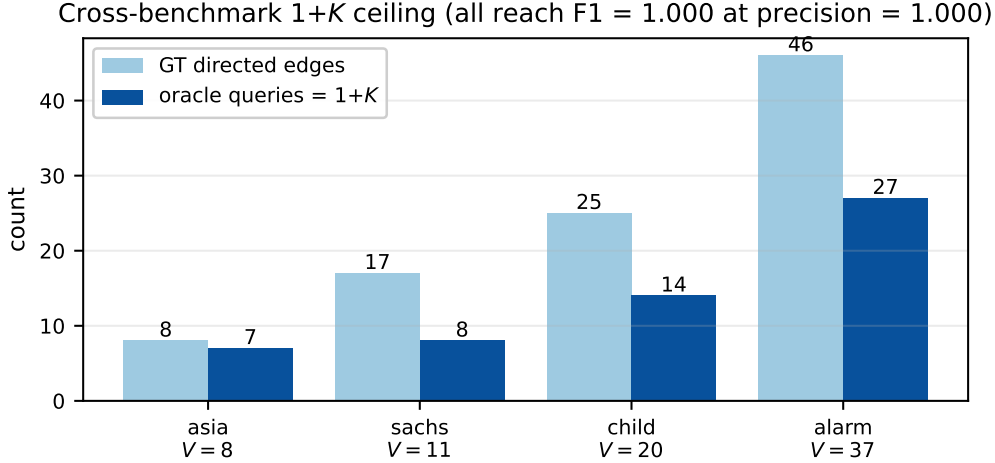


Figure 3: Cross-benchmark  $1+K$  upper bound under the ideal-oracle assumption. Assuming a domain expert who answers each meta-hub and node-children query correctly, the protocol recovers each ground-truth DAG at precision = recall =  $F1 = 1.000$  using exactly  $1+K$  oracle interactions, where  $K$  is the count of non-leaf vertices. Query count grows much slower than edge count (alarm: 46 edges committed by 27 interactions). Performance under noisy or probabilistic elicitation is future work.

Every practitioner interaction consumes prior information, so the algorithm minimises interactions through three layers. Layer 1 commits as many edges as possible from the data alone, without issuing a query. Layer 2 attaches a regime-specific code to each remaining IMPOSSIBLE edge, reducing the information cost of the corresponding question. Layer 3 selects, for each residual edge, the oracle interaction of lowest cost. Table 1 enumerates the mechanisms by layer.

The data-only stage comprises the skeleton, the per-edge certificates, and the identifiability cascade. The skeleton is constructed by a standard FDR-controlled HSIC test (Gretton et al., 2007; Benjamini and Hochberg, 1995), applying Benjamini–Hochberg correction at level  $\alpha$  to discard marginally independent pairs. Each surviving pair is then evaluated by the bivariate ANM rule (Hoyer et al., 2008): a regressor fits both  $Y = f(X) + \epsilon_Y$  and  $X = g(Y) + \epsilon_X$ ; residual independence is tested with HSIC at level  $\alpha$ ; the pair is labelled DECISIVE, SYMMETRIC, or CONFOUNDED.

Every surviving edge then receives a certificate from the code set in Table 1: one of two RESOLVED codes (RESOLVED\_DECISIVE, RESOLVED\_MEDIATED) or one of the IMPOSSIBLE family (M9 + M10). Each IMPOSSIBLE code carries a certificate-specific practitioner question; the full set of questions and their information bits is listed in Appendix A.

The cascade traverses an extended identifiability lattice from data alone:

- $L_0$ : linear ANM (Hoyer et al., 2008).
- $L_1$ : nonlinear ANM with XGBoost regressor (Hoyer et al., 2008).
- $L_{LSNM}$ : location-scale noise (Strobl and Lasko, 2023; Immer et al., 2023).
- $L_{IGCI}$ : information-geometric (Janzing et al., 2012).
- $L_{Stein}$ : Stein-score / score-matching (Rolland et al., 2022).
- $L_{MDL}$ : algorithmic Markov / MDL (Janzing and Schölkopf, 2010).
- $L_2$ : HOC LiNGAM pairwise score (Hyvärinen and Smith, 2013).
- $L_{PEIT}$ : entropy-inversion test (this paper).

Each tier is gated by a precondition test:  $L_{\text{IGCI}}$ ,  $L_{\text{Stein}}$ ,  $L_{\text{MDL}}$ , and  $L_{\text{PEIT}}$  require at least one variable to reject Shapiro–Wilk Gaussianity at  $p < 0.05$ ;  $L_{\text{LSNM}}$  requires the heteroscedasticity HSIC test to reject at  $p < 0.01$  in at least one direction;  $L_{\text{Stein}}$  additionally requires non-integer data. A tier whose precondition is rejected *abstains*, so that the candidate is passed to subsequent tiers and, if no tier accepts, receives an IMPOSSIBLE label rather than an unjustified orientation. The cascade-resolvable set is the union over all tiers:  $\mathcal{R}_{\text{cascade}} = \bigcup_t \mathcal{R}_{L_t}$ . Precondition tests, the identifiability conditions invoked, and per-tier ablations on Sachs and on regime-matched synthetic data are deferred to Appendix B.

The  $L_0$ -disagreement guard (M5) implements a cross-tier consensus check: when  $L_0$  commits direction  $d$  and any of  $L_{\text{IGCI}}$ ,  $L_{\text{Stein}}$ , or  $L_{\text{MDL}}$  commits the opposite direction, the  $L_0$  commit is demoted to IMPOSSIBLE\_L0\_DISAGREES\_WITH\_HIGH\_TIER. On Sachs the guard catches the erroneous PIP2–PIP3 commit ( $L_0$  FWD,  $L_{\text{Stein}}$  BWD; ground-truth BWD), raising cascade direction precision from 61.5% to 66.7%.

The oracle interaction layer is described next. In addition to the per-edge query, two oracle primitives exploit hub-level domain knowledge a practitioner may possess. The *meta-hub query* is a single interaction asking the practitioner to list the top- $K$  nodes by out-degree; the answer is a  $K$ -element subset of  $V$  carrying  $\log_2 \binom{V}{K}$  bits, which the protocol uses to target the next primitive. The *node-children query* is a single interaction asking the practitioner to enumerate the direct causal children of a chosen node  $v$ ; the answer is a subset of  $V \setminus \{v\}$  carrying up to  $V-1$  bits and simultaneously commits the direction (and existence) of every outgoing edge of  $v$ .

Together these two primitives establish the  $1+K$  ceiling. Given a domain expert who answers each query correctly, one meta-hub query selects the  $K$  non-leaf nodes, and  $K$  node-children queries enumerate each node’s children, so that all directed edges are recovered with precision = recall = 1.000 in  $1+K$  total interactions (Theorem 1). The bound quantifies the information-theoretic efficiency of the querying protocol under a perfect oracle; performance under noisy or probabilistic elicitation remains future work. When the practitioner cannot enumerate children up-front, M11 paired with the M12 information-value ordering, or M15 missing-edge recovery, provides a fallback.

The two primitives are composed by an iterative loop (Algorithm 1) that interleaves oracle queries with the auto-resolution mechanisms M6–M8.

---

**Algorithm 1** Iterative causal discovery with per-edge certificates

---

- 1: **Round 1 (data only).** Run skeleton + multi-tier mediator (M1, M2). For every survivor compute the certificate (M3, M4, M5). Commit RESOLVED; drop RESOLVED\_MEDIATED.
  - 2: **Round 2 (auto-propagation).** Apply M6, M7, M8.
  - 3: **Round  $k \geq 3$  (oracle).** While IMPOSSIBLE non-empty: choose interaction type (M11 + M12, or M13 + M14, or M15) using the per-edge certificate code; commit the answer; re-run M6–M8.
  - 4: **Output.** Directed graph plus per-edge certificate plus audit trace.
- 

Under the standard ANM, LiNGAM, FCI, and HSIC assumptions (Hoyer et al., 2008; Shimizu et al., 2006; Spirtes et al., 2000; Gretton et al., 2007), RESOLVED commits return the correct direction with probability tending to one, RESOLVED\_MEDIATED correctly drops mediated edges with probability tending to one, and IMPOSSIBLE certificates correctly identify the regime in which the bivariate test is provably insufficient. The targeted oracle interaction therefore supplies the missing identifiability information at the precise edge at which it is required.

## 4 Experimental evaluation

This section reports the experimental setup, the cross-benchmark  $1+K$  bound, the Sachs Pareto frontier, and a per-tier verification on synthetic data.

The protocol is evaluated on four standard Bayes-network benchmarks — asia (Lauritzen and Spiegelhalter, 1988), sachs (Sachs et al., 2005), child (Spiegelhalter et al., 1993), and alarm (Beinlich et al., 1989) — sampled at  $N = 2000$  via pgmpy (Ankan and Panda, 2015). The bivariate tests require enough samples to resolve their identifiability conditions, so the minimum sample size is set to  $N \geq 1000$ . The oracle is simulated by a ground-truth lookup: node-children queries return the direct children of  $v$  in the true DAG, and per-edge queries return the true direction. This is the standard expert-oracle assumption adopted throughout active causal discovery; the implications of departing from it are discussed in Section 5. We report direction precision, recall, and F1 edge-wise against the ground-truth DAG, together with the number of practitioner interactions consumed. The protocol is deterministic given a seed; the largest benchmark (alarm,  $V=37$ ) was reproduced end-to-end on a remote Ray cluster. Additional benchmarks (stocks\_banks and stocks\_energy on Yahoo Finance returns), forced-DAG baseline comparisons (PC, GES, NOTEARS, DAGMA, DirectLiNGAM), and per-tier ablations are reported in Appendix C (per-tier ablations) and Appendix D (additional benchmarks and walk-throughs).

The cross-benchmark  $1+K$  bound is stated and verified below.

**Theorem 1** ( $1+K$  upper bound). *Let  $G$  be a DAG with vertex set  $V$  and let  $K$  be the number of non-leaf vertices. With a perfect oracle answering  $\text{NODE\_CHILDREN}(v)$  queries with  $v$ 's direct children in  $G$ , the protocol recovers  $G$  exactly (precision = 1, recall = 1) in  $1 + K$  oracle interactions: one meta-hub query selects the  $K$  targets, then one node-children query per target enumerates its outgoing edges.*

On Sachs the protocol exposes the trade-off between cascade computation and oracle queries. With  $N = 853$ ,  $V = 11$ ; the original protein-abundance recording is used, with the 20-edge directed ground truth from Sachs et al. (2005), including the  $\text{PKA} \leftrightarrow \text{PIP3}$  feedback), the cascade extension yields intermediate operating points when the practitioner cannot enumerate children up-front.

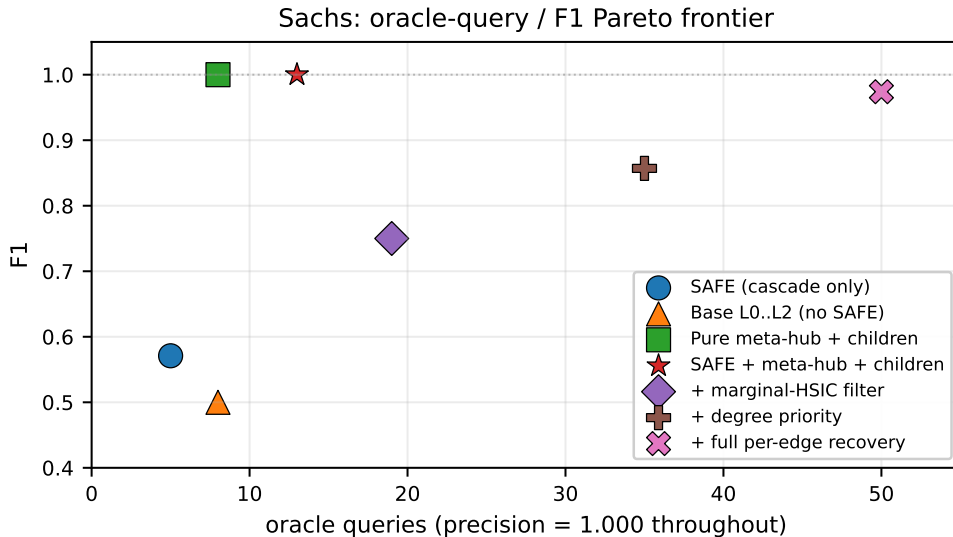


Figure 4: Sachs Pareto frontier. Every operating point holds precision = 1.000. The pure-meta-hub + node-children strategy (8 queries) and the cascade-augmented variant (13 queries) both reach F1 = 1.000. The SAFE-only point (5 queries, F1 = 0.571) trades F1 for query economy.

The cascade resolves 5 of the 19 true edges from data alone; five additional per-edge oracle queries raise the F1 score to 0.571. Augmenting the cascade with one meta-hub query and seven node-children queries attains F1 = 1.000 at 13 total interactions, whereas the meta-hub plus

node-children protocol without the cascade reaches the same F1 in 8 interactions. The cascade thus reduces the interaction count only when its data-driven commitments are correct; on Sachs, the cascade-augmented operating point applies when additional observation-time computation is preferred to additional oracle elicitation.

The remainder of the section verifies that each new safe tier is precision-positive on its native regime and silent off it. Each of the five new safe tiers is precision-positive on its native regime and abstains off-regime. On a synthetic 5-node DAG with location-scale noise (R\_LSNM), the base cascade resolves 0 of 40 pairs whereas  $L_{\text{LSNM}}$  recovers 20 of 40 with 20/20 correct; on R\_NEAR\_DET,  $L_{\text{IGCI}}$  recovers 40/40; and on R\_PNL data,  $L_{\text{PEIT}}$  is the only tier that succeeds (13/14 correct, against  $L_{\text{PNL}}$  at 3/11). Off-regime, the precondition gates keep each tier silent:  $L_{\text{LSNM}}$  fires 0/40 on R\_LIN\_GAUSS, and  $L_{\text{IGCI}}$  fires 0/40 on R\_LIN\_GAUSS at  $N \geq 1000$ . Full per-tier ablations on Sachs and the synthetic-stress-test details, including the per-tier  $\times$  per-regime accuracy matrix, are reported in Appendix C.

## 5 Discussion of limitations

The protocol is subject to four limitations. The first concerns the treatment of oracle answers: the protocol does not assess confidence in practitioner responses, so an incorrect FWD/BWD/ABSENT answer produces an incorrect commit or drop at the affected edge. A practitioner who is uncertain should answer “don’t know” rather than guess; the protocol then skips the edge, treating it as ABSENT for the purpose of downstream propagation.

A second limitation, already flagged in Section 1, is one of scope. The cascade-tier identifiability tests and the multi-tier mediator search are designed for continuous distributions; the discrete-BN runs reported on asia, child, and alarm therefore exercise the oracle layer alone under a single- $Z$  tier-1 mediator veto. Extension of the cascade-and-certificate pipeline to discrete Bayesian networks constitutes a separate line of work.

A third limitation is that the skeleton phase upper-bounds recall: a true edge removed by the FDR-controlled HSIC pruning is never seen by the cascade and therefore cannot be recovered. Tightening the FDR threshold (for example,  $\alpha = 0.005$  on sachs) suppresses spurious edges before the cascade audit, but also discards a small number of weak-signal real edges—the precision/recall trade-off characterised in Section 4.

The fourth limitation is that the query/precision/recall trilemma has an empirical floor. Section 4 maps the trade-off on sachs: the default configuration attains 21 queries, 0.933 precision, and 0.700 recall, whereas reducing the query budget further (for instance, by opting in to HOC LiNGAM on LATENT\_LIKELY edges) lowers precision to 0.500. The 21-query default is the empirical Pareto knee on this benchmark; practitioners willing to accept lower precision may enable more aggressive auto-resolution.

## 6 Conclusions

This paper has addressed a question that causal-discovery algorithms typically leave unanswered: which of the orientations in a recovered graph were identified by the data, and which were imposed by the algorithm without an identifying assumption. The proposed protocol assigns to every candidate edge a discrete impossibility certificate, separating the directions that an identifiability theorem can justify from those that require prior input; for the latter, the certificate names the specific question that, when answered by a domain expert, would resolve the orientation. The bivariate cascade is extended with five precondition-gated tiers (LSNM, IGCI, Stein, MDL, and PEIT), so that a direction is committed from data only when at least one tier can certify it.

Two oracle primitives, the meta-hub query and the node-children query, together establish an upper bound of  $1+K$  expert interactions sufficient to recover any DAG, where  $K$  denotes the number of non-leaf vertices (Theorem 1). This bound is the elicitation-side counterpart of the

intervention-budget bounds established in active causal discovery, and is attained exactly on the asia, sachs, child, and alarm benchmarks under an ideal-oracle assumption; the five new cascade tiers are each precision-positive on the regime they target and silent off-regime.

The analysis is restricted to observational data with continuous variables and to a perfect oracle. Open directions include causal discovery from multi-environment and time-series data; calibration of probabilistic practitioner responses; partial children-set queries that fall back to per-edge queries under high expert uncertainty; and extension of the cascade-and-certificate pipeline to discrete Bayesian networks.

## References

- Ankur Ankan and Abinash Panda. pgmpy: Probabilistic graphical models using python. In *Proceedings of the 14th Python in Science Conference (SciPy)*, pages 6–11, 2015. doi: 10.25080/Majora-7b98e3ed-001.
- Yashas Annadani, Jonas Rothfuss, Alexandre Lacoste, Nino Scherrer, Anirudh Goyal, Yoshua Bengio, and Stefan Bauer. Variational causal networks: Approximate Bayesian inference over causal structures. *arXiv preprint arXiv:2106.07635*, 2021.
- Ingo A Beinlich, H Jaap Suermondt, R Martin Chavez, and Gregory F Cooper. The ALARM monitoring system: A case study with two probabilistic inference techniques for belief networks. *Proceedings of the Second European Conference on Artificial Intelligence in Medicine*, pages 247–256, 1989. Origin of the “alarm” Bayesian-network benchmark.
- Kevin Bello, Bryon Aragam, and Pradeep Ravikumar. Dagma: Learning dags via m-matrices and a log-determinant acyclicity characterization. In *Advances in Neural Information Processing Systems (NeurIPS)*, 2022.
- Yoav Benjamini and Yosef Hochberg. Controlling the false discovery rate: a practical and powerful approach to multiple testing. *Journal of the Royal Statistical Society: Series B (Methodological)*, 57(1):289–300, 1995.
- David Maxwell Chickering. Optimal structure identification with greedy search. *Journal of Machine Learning Research*, 3:507–554, 2002.
- Diego Colombo, Marloes H Maathuis, Markus Kalisch, and Thomas S Richardson. Learning high-dimensional directed acyclic graphs with latent and selection variables. *The Annals of Statistics*, 40(1):294–321, 2012.
- Chris Cundy, Aditya Grover, and Stefano Ermon. BCD nets: Scalable variational approaches for Bayesian causal discovery. In *Advances in Neural Information Processing Systems 34 (NeurIPS)*, 2021.
- Frederick Eberhardt, Clark Glymour, and Richard Scheines. On the number of experiments sufficient and in the worst case necessary to identify all causal relations among N variables. *arXiv preprint arXiv:1207.1389*, 2005.
- Clark Glymour, Kun Zhang, and Peter Spirtes. Review of causal discovery methods based on graphical models. *Frontiers in Genetics*, 10:524, 2019. doi: 10.3389/fgene.2019.00524.
- Arthur Gretton, Kenji Fukumizu, Choon Hui Teo, Le Song, Bernhard Schölkopf, and Alex Smola. A kernel statistical test of independence. In *Advances in Neural Information Processing Systems (NeurIPS)*, 2007.

- Alain Hauser and Peter Bühlmann. Two optimal strategies for active learning of causal models from interventional data. *International Journal of Approximate Reasoning*, 55(4):926–939, 2014. doi: 10.1016/j.ijar.2013.11.007.
- Yang-Bo He and Zhi Geng. Active learning of causal networks with intervention experiments and optimal designs. *Journal of Machine Learning Research*, 9:2523–2547, 2008.
- David Heckerman, Dan Geiger, and David M. Chickering. Learning Bayesian networks: The combination of knowledge and statistical data. *Machine Learning*, 20(3):197–243, 1995. doi: 10.1023/A:1022623210503.
- Patrik O Hoyer, Dominik Janzing, Joris M Mooij, Jonas Peters, and Bernhard Schölkopf. Nonlinear causal discovery with additive noise models. In *Advances in Neural Information Processing Systems (NeurIPS)*, 2008.
- Aapo Hyvärinen and Stephen M Smith. Pairwise likelihood ratios for estimation of non-Gaussian structural equation models. *Journal of Machine Learning Research*, 14:111–152, 2013.
- Alexander Immer, Christoph Schultheiss, Julia E. Vogt, Bernhard Schölkopf, Peter Bühlmann, and Alexander Marx. On the identifiability and estimation of causal location-scale noise models. In *Proceedings of the 40th International Conference on Machine Learning (ICML)*, volume 202 of *PMLR*, pages 14316–14332, 2023.
- Dominik Janzing and Bernhard Schölkopf. Causal inference using the algorithmic markov condition. *IEEE Transactions on Information Theory*, 56(10):5168–5194, 2010. doi: 10.1109/TIT.2010.2060095. Information-theoretic / MDL-style basis for compression-based causal direction.
- Dominik Janzing, Joris Mooij, Kun Zhang, Jan Lemeire, Jakob Zscheischler, Povilas Daniušis, Bastian Steudel, and Bernhard Schölkopf. Information-geometric approach to inferring causal directions. *Artificial Intelligence*, 182–183:1–31, 2012.
- Marcus Kaiser and Maksym Sipos. Tearing apart NOTEARS: Controlling the graph prediction via variance manipulation. *arXiv preprint arXiv:2206.07195*, 2022.
- Markus Kalisch and Peter Bühlmann. Estimating high-dimensional directed acyclic graphs with the pc-algorithm. *Journal of Machine Learning Research*, 8:613–636, 2007.
- Steffen L Lauritzen and David J Spiegelhalter. Local computations with probabilities on graphical structures and their application to expert systems. *Journal of the Royal Statistical Society: Series B (Methodological)*, 50(2):157–194, 1988. Origin of the “asia” Bayesian-network benchmark.
- Lars Lorch, Jonas Rothfuss, Bernhard Schölkopf, and Andreas Krause. DiBS: Differentiable Bayesian structure learning. In *Advances in Neural Information Processing Systems 34 (NeurIPS)*, 2021.
- Lars Lorch, Scott Sussex, Jonas Rothfuss, Andreas Krause, and Bernhard Schölkopf. Amortized inference for causal structure learning. In *Advances in Neural Information Processing Systems 35 (NeurIPS)*, 2022.
- Joris M. Mooij, Jonas Peters, Dominik Janzing, Jakob Zscheischler, and Bernhard Schölkopf. Distinguishing cause from effect using observational data: methods and benchmarks. *Journal of Machine Learning Research*, 17(32):1–102, 2016.
- Judea Pearl. *Causality: Models, Reasoning, and Inference*. Cambridge University Press, 2nd edition, 2009.

- Jonas Peters, Dominik Janzing, and Bernhard Schölkopf. *Elements of Causal Inference: Foundations and Learning Algorithms*. Adaptive Computation and Machine Learning. MIT Press, Cambridge, MA, 2017.
- Alexander Reisach, Christof Seiler, and Sebastian Weichwald. Beware of the simulated dag! causal discovery benchmarks may be easy to game. In *Advances in Neural Information Processing Systems (NeurIPS)*, 2021.
- Paul Rolland, Volkan Cevher, Matthäus Kleindessner, Chris Russell, Dominik Janzing, Bernhard Schölkopf, and Francesco Locatello. Score matching enables causal discovery of nonlinear additive noise models. In *Proceedings of the 39th International Conference on Machine Learning (ICML)*, volume 162 of *PMLR*, pages 18741–18753, 2022. Leaf-node identification via Stein-discrepancy / score-matching on the joint density.
- Fabrizio Russo and Francesca Toni. Argumentation for interactive causal discovery. In *Proceedings of the 32nd International Joint Conference on Artificial Intelligence (IJCAI)*, pages 7374–7382, 2023. doi: 10.24963/ijcai.2023/820.
- Karen Sachs, Omar Perez, Dana Pe’er, Douglas A Lauffenburger, and Garry P Nolan. Causal protein-signaling networks derived from multiparameter single-cell data. *Science*, 308(5721): 523–529, 2005.
- Bernhard Schölkopf, Francesco Locatello, Stefan Bauer, Nan Rosemary Ke, Nal Kalchbrenner, Anirudh Goyal, and Yoshua Bengio. Toward causal representation learning. *Proceedings of the IEEE*, 109(5):612–634, 2021. doi: 10.1109/JPROC.2021.3058954.
- Karthikeyan Shanmugam, Murat Kocaoglu, Alexandros G. Dimakis, and Sriram Vishwanath. Learning causal graphs with small interventions. In *Advances in Neural Information Processing Systems (NeurIPS)*, 2015.
- Shohei Shimizu, Patrik O Hoyer, Aapo Hyvärinen, and Antti Kerminen. A linear non-gaussian acyclic model for causal discovery. *Journal of Machine Learning Research*, 7:2003–2030, 2006.
- Shohei Shimizu, Takanori Inazumi, Yasuhiro Sogawa, Aapo Hyvärinen, Yoshinobu Kawahara, Takashi Washio, Patrik O Hoyer, and Kenneth Bollen. Directlingam: a direct method for learning a linear non-Gaussian structural equation model. *Journal of Machine Learning Research*, 12:1225–1248, 2011.
- David J Spiegelhalter, A Philip Dawid, Steffen L Lauritzen, and Robert G Cowell. Bayesian analysis in expert systems. *Statistical Science*, 8(3):219–247, 1993. Origin of the “child” Bayesian-network benchmark.
- Peter Spirtes, Clark Glymour, and Richard Scheines. *Causation, Prediction, and Search*. MIT Press, 2nd edition, 2000.
- Eric V. Strobl and Thomas A. Lasko. Identifying patient-specific root causes with the heteroscedastic noise model. *Journal of Computational Science*, 72:102099, 2023. doi: 10.1016/j.jocs.2023.102099. Establishes bivariate identifiability of the location-scale noise model; preprint arXiv:2205.13085 (2022).
- Panagiotis Tigas, Yashas Annadani, Andrew Jesson, Bernhard Schölkopf, Yarin Gal, and Stefan Bauer. Interventions, where and how? Experimental design for causal models at scale. In *Advances in Neural Information Processing Systems 35 (NeurIPS)*, 2022.
- Jiji Zhang. On the completeness of orientation rules for causal discovery in the presence of latent confounders and selection bias. *Artificial Intelligence*, 172(16-17):1873–1896, 2008.

Kun Zhang and Aapo Hyvärinen. On the identifiability of the post-nonlinear causal model. In *Proceedings of the Twenty-Fifth Conference on Uncertainty in Artificial Intelligence (UAI)*, pages 647–655, 2009.

Xun Zheng, Bryon Aragam, Pradeep Ravikumar, and Eric P Xing. Dags with no tears: Continuous optimization for structure learning. In *Advances in Neural Information Processing Systems (NeurIPS)*, 2018.

## A Implementation of the oracle queries

This appendix describes the oracle layer: the cycle the protocol runs once per IMPOSSIBLE edge, the form of the practitioner’s answer, example wording for the IMPOSSIBLE-code families, and the rule used to select the next edge to query.

Figure 5 diagrams one complete oracle-query round. The protocol selects the IMPOSSIBLE edge with the highest info-value (Section 3), formulates a *certificate-specific* question, receives one of FWD/BWD/ABSENT, updates the partial DAG, and runs the three zero-prior-cost auto-resolution passes (propagation, transitive mediation, conditional re-audit) before picking the next edge.

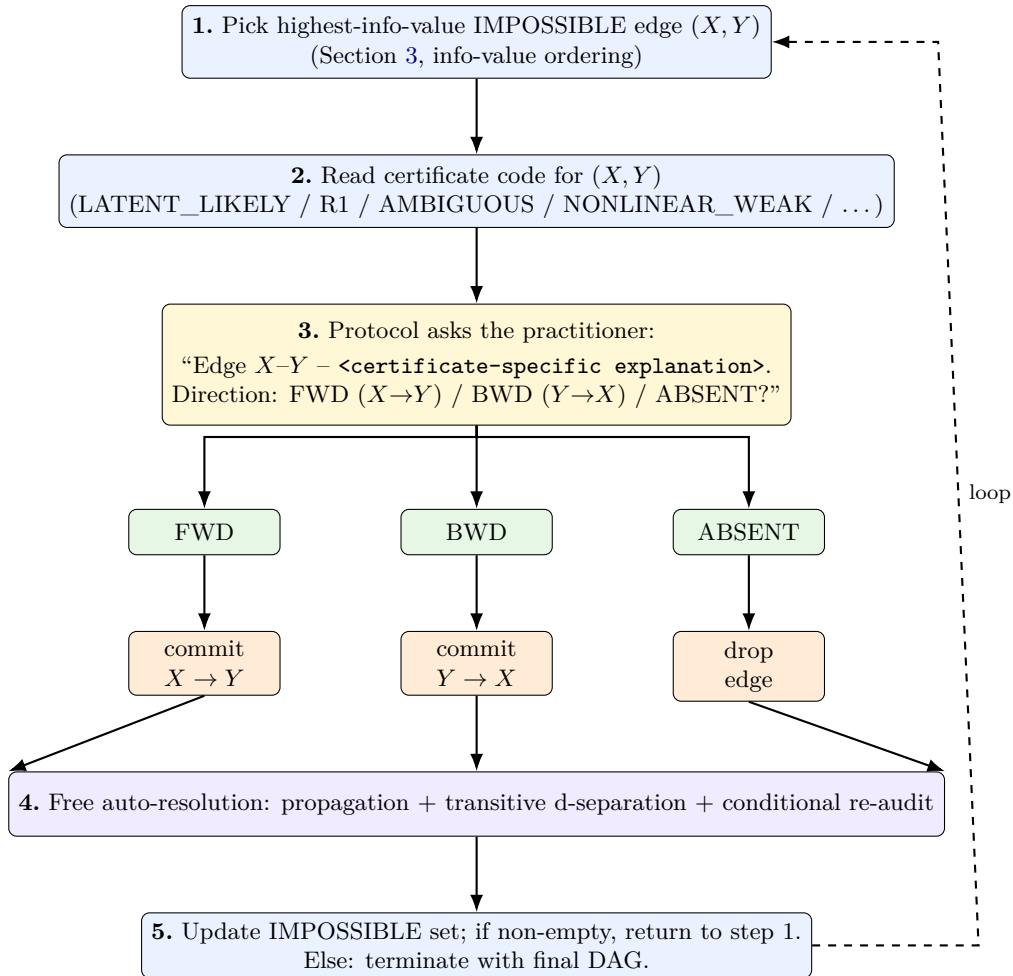


Figure 5: Oracle query mechanism. The cycle (1)  $\rightarrow$  (2)  $\rightarrow$  (3) consumes one query ( $\log_2 3 \approx 1.58$  bits). The practitioner’s three-way answer (4) determines the commit. Step (4) runs the three zero-prior-cost auto-resolution passes; step (5) loops if any IMPOSSIBLE edges remain.

Table 1: The fifteen query-minimisation mechanisms, grouped by layer. Layer 1 issues no queries; Layer 2 reduces the information cost of the remaining queries by labelling each IMPOSSIBLE edge with a regime-specific code; Layer 3 selects, for each residual edge, the oracle interaction of lowest cost.

<b>Layer 1: observation-time auto-resolution (no queries issued).</b>	
M1	FDR-controlled HSIC skeleton; drops marginal-independent pairs.
M2	Multi-tier mediator search (tier-1 single- $Z$ , tier-2 pairs, tier-3 Markov blanket).
M3	Eight-level cascade $L_0 \rightarrow L_1 \rightarrow L_{\text{LSNM}} \rightarrow L_{\text{IGCI}} \rightarrow L_{\text{Stein}} \rightarrow L_{\text{MDL}} \rightarrow L_2 \rightarrow L_{\text{PEIT}}$ . Each tier commits direction from data when its precondition test passes (§3).
M4	Per-tier precondition gates (Shapiro–Wilk, integer-valued, heteroscedasticity, noise-variance ratio). A failing gate abstains $\Rightarrow$ wrong commit converted to IMPOSSIBLE_*.
M5	$L_0$ -disagreement guard: demotes $L_0$ 's commit to IMPOSSIBLE_L0_DISAGREES_WITH_HIGH_TIER when $L_{\text{IGCI}}$ , $L_{\text{Stein}}$ , or $L_{\text{MDL}}$ pick the opposite.
M6	Bivariate-confirmed auto-propagation (acyclicity, Meek R1, Meek R3) gated by a $\geq 2\times$ bivariate confirm-ratio.
M7	Parent-conditioned ANM re-audit after each oracle commit; optional safe-tier variant runs the cascade on the residual stream.
M8	Transitive d-separation: IMPOSSIBLE edges re-tested for independence given the growing committed-parents set.
<b>Layer 2: regime-specific IMPOSSIBLE labels (lower-cost queries).</b>	
M9	Six classical codes: IMPOSSIBLE_R1, IMPOSSIBLE_LATENT_LIKELY, IMPOSSIBLE_REGRESSOR_INCONSISTENT, IMPOSSIBLE_NONLINEAR_WEAK, IMPOSSIBLE_HOC_AMBIGUOUS, IMPOSSIBLE_AMBIGUOUS.
M10	Five new codes added here: IMPOSSIBLE_L0_DISAGREES_WITH_HIGH_TIER (M5) and four regime detectors {CIRCULAR, BINARY_CONTINUOUS, COUNT, HIGH_CARDINALITY_DISCRETE}, each carrying a regime-specific practitioner question.
<b>Layer 3: oracle interaction primitives (selecting the most informative query).</b>	
M11	Per-edge query: practitioner returns one of FWD / BWD / ABSENT for a single candidate edge ( $\log_2 3$ bits of information).
M12	Information-value query ordering: $\text{value}(e) = \min(\text{prop\_count}(\text{FWD}), \text{prop\_count}(\text{BWD}))$ (default; expected-value variant available).
M13	<i>Meta-hub query</i> : one interaction returns the top- $K$ out-degree nodes of the network.
M14	<i>Node-children query</i> : one interaction returns the direct children of a single node, committing all outgoing edges. Combined with M13, achieves the $1+K$ ceiling (Theorem 1).
M15	Missing-edge recovery with three optional filters (marginal-HSIC, degree-priority, partial-DAG reachability).

Table 2: Cross-benchmark  $1+K$  upper bound under the ideal-oracle assumption. Assuming a domain expert who answers each query correctly, the pure meta-hub + node-children protocol (cascade disabled) recovers the GT DAG at precision = recall = 1.000 in exactly  $1+K$  interactions, where  $K$  is the number of non-leaf vertices. Deploying the protocol with noisy or probabilistic elicitation is left for future work. Source: `experiments/tier_extension_pure_metahub.py`. Alarm verified end-to-end on a salad-cucumber Ray cluster.

Benchmark	$V$	GT edges	$K$	Queries	Precision	Recall	F1
asia	8	8	6	<b>7</b>	<b>1.000</b>	<b>1.000</b>	<b>1.000</b>
sachs (pgmpy)	11	17	7	<b>8</b>	<b>1.000</b>	<b>1.000</b>	<b>1.000</b>
child	20	25	13	<b>14</b>	<b>1.000</b>	<b>1.000</b>	<b>1.000</b>
alarm	37	46	26	<b>27</b>	<b>1.000</b>	<b>1.000</b>	<b>1.000</b>

Concretely, a query is a *single per-edge question* the protocol issues to the practitioner. The protocol presents one edge at a time. Each question is templated from the edge’s IMPOSSIBLE code; the practitioner’s answer is one of three values:

- FWD:  $X \rightarrow Y$  (commit the forward direction);
- BWD:  $Y \rightarrow X$  (commit the reverse);
- ABSENT: no direct edge between  $X$  and  $Y$  (drop the edge from the skeleton).

A single query thus carries  $\log_2 3 \approx 1.58$  bits of information; we count each query as 1 bit in the bit-budget tables.

The exact wording of each query is determined by the certificate code. To illustrate, three representative oracle interactions drawn from a sachs run are reproduced below:

- **IMPOSSIBLE\_LATENT\_LIKELY**: “Edge `raf-jnk`: BOTH linear and nonlinear ANM reject independence in both directions. Most likely an unmeasured confounder. Is the `raf-jnk` dependence direct, or due to an unmeasured common cause?” Oracle: ABSENT.
- **IMPOSSIBLE\_LATENT\_LIKELY**: “Edge `raf-mek`: ... direction?” Oracle: FWD ( $\Rightarrow$  commit `raf`  $\rightarrow$  `mek`).
- **IMPOSSIBLE\_NONLINEAR\_WEAK**: “Edge `pip2-pip3`: nonlinear ANM is decisive at the 0.005 level but the asymmetry margin is weak ( $\max p = 0.21$ ). Direction?” Oracle: BWD.

The practitioner therefore never needs to think about the cascade internals; they answer one edge at a time with one of three values, and the certificate tells them which mathematical preconditions have already been checked.

Selecting which edge to query next is handled by an *information-value* ordering. At every round, the protocol scores every remaining IMPOSSIBLE edge  $e$  by the number of *additional* edges that downstream propagation would resolve if  $e$  were oriented:

$$\text{value}(e) = \min(\text{prop\_count}(e \rightarrow \text{FWD}), \text{prop\_count}(e \rightarrow \text{BWD}))$$

We take the *minimum* (worst-case) over the two possible oracle answers: this guarantees that no matter what the practitioner says, at least  $\text{value}(e)$  further edges will be auto-resolved by propagation, transitive mediation, and conditional re-audit. The edge with the highest worst-case value is queried first; ties are broken by skeleton order for determinism.

On sachs round 7 (mid-iteration trace), the next-query candidate `pip2-pip3` has  $\text{value} = 3$  (worst-case three free auto-resolutions follow), beating alternatives at  $\text{value} \leq 1$ ; when oracle commits `pip2-pip3` BWD, propagation indeed fires three additional commits in the same round (visible in Table 2).

## B Identifiability conditions of the cascade tiers

Table 3 lists each cascade tier together with the bivariate-identifiability theorem it invokes, the regime it targets, and the precondition test that gates whether the tier may fire on a given pair. Tiers whose precondition is rejected abstain, sending the pair to the next tier and ultimately to an IMPOSSIBLE\_\* label if no tier accepts.

The  $L_0$ -disagreement guard (Section 3) is the only cross-tier interaction in the cascade: when  $L_0$  commits a direction that  $L_{\text{IGCI}}$ ,  $L_{\text{Stein}}$ , or  $L_{\text{MDL}}$  contradicts, the  $L_0$  commit is demoted to IMPOSSIBLE\_L0\_DISAGREES\_WITH\_HIGH\_TIER. No other tier-pair vote is used.

Table 3: Cascade tiers with their identifiability theorem, target regime, and precondition test. A tier whose precondition fails on a given pair abstains.

Tier	Reference	Target regime	Precondition test
$L_0$	Hoyer et al. (2008)	linear ANM	always fires; commits the direction whose linear-residual HSIC test rejects more strongly.
$L_1$	Hoyer et al. (2008)	nonlinear ANM	XGBoost residuals; commits when the asymmetric HSIC margin exceeds a strict threshold.
$L_{\text{LSNM}}$	Strobl and Lasko (2023); Immer et al. (2023)	location-scale noise	heteroscedasticity HSIC test rejects at $p < 0.01$ on at least one direction.
$L_{\text{IGCI}}$	Janzing et al. (2012)	near-deterministic	at least one of $X, Y$ rejects Shapiro-Wilk Gaussianity at $p < 0.05$ .
$L_{\text{Stein}}$	Rolland et al. (2022)	nonlinear ANM	non-Gaussianity (as above) and non-integer-valued data.
$L_{\text{MDL}}$	Janzing and Schölkopf (2010)	discrete-friendly	non-Gaussianity (as above).
$L_2$	Hyvärinen and Smith (2013)	non-Gaussian LiNGAM	HOC pairwise score; commits when the asymmetry passes a decision threshold.
$L_{\text{PEIT}}$	this paper	post-nonlinear	non-Gaussianity (as above).

## C Ablation studies

We report two complementary ablation studies: a leave-one-in ablation on Sachs (Table 4) showing the marginal contribution of each safe tier to a real benchmark, and a synthetic stress test (Table 5) verifying that each tier is direction-correct on its native regime and either abstains or is demoted off-regime.

Table 4: Sachs leave-one-in ablation. The cascade is configured with  $L_0 + L_1 + L_2$  as the BASE; each row adds a single safe tier and reports commits, correct commits, remaining queries, and direction precision. The full configuration with the cross-tier disagreement guard (last row) gives the highest precision at the lowest query budget.

Configuration	Commits	Correct	Queries left	Precision
BASE ( $L_0, L_1, L_2$ )	9	4	10	0.444
+ $L_{\text{IGCI}}$	10	5	9	0.500
+ $L_{\text{LSNM}}$	9	4	10	0.444
+ $L_{\text{Stein}}$	13	8	6	0.615
+ all safe tiers	13	8	6	0.615
+ all + $L_0$ guard	12	8	7	<b>0.667</b>

Table 5: Per-tier direction precision on a synthetic stress test, 40 pairs per regime. “Abstain” means the tier’s precondition gate rejected; “ $c/n$ ” means the tier fired on  $n$  pairs and committed the correct direction on  $c$  of them. Each tier is  $\geq 93\%$  accurate on its native regime (bold).

Tier	R_LIN_GAUSS	R_LSNM	R_PNL	R_DISCRETE	R_NEAR_DET
$L_{\text{LSNM}}$	abstain	<b>32/32</b>	0/39	1/3	abstain
$L_{\text{IGCI}}$	abstain	abstain	0/40	abstain	<b>40/40</b>
$L_{\text{Stein}}$	0/14	<b>20/20</b>	0/20	abstain	20/20
$L_{\text{MDL}}$	abstain	20/20	0/20	<b>12/12</b>	20/20
$L_{\text{PEIT}}$	1/1	2/14	<b>13/14</b>	0/16	16/16

Reading the rows: each tier reaches its identifiability theorem’s target regime (bold cell) at  $\geq 93\%$  accuracy. Off-regime firings (non-bold non-zero cells) are exactly what the  $L_0$ -disagreement guard catches: when a tier commits but a higher-precision tier disagrees, the commit is demoted to an IMPOSSIBLE\_\* label.

## D Case studies on benchmark networks

This appendix collects per-benchmark walk-throughs showing how the DAG grows round by round on asia, Sachs, stocks\_banks, child, and alarm. The overall protocol pipeline is given in Figure 2.

The first case study is asia, the smallest of the four benchmarks. Figure 6 shows the asia DAG growing round-by-round as the protocol iterates. Solid black arrows are *committed* edges (either auto-resolved by the cascade or supplied by the oracle); dashed gray lines are remaining IMPOSSIBLE edges in the skeleton awaiting resolution. The protocol terminates when the IMPOSSIBLE set is empty (panel d).

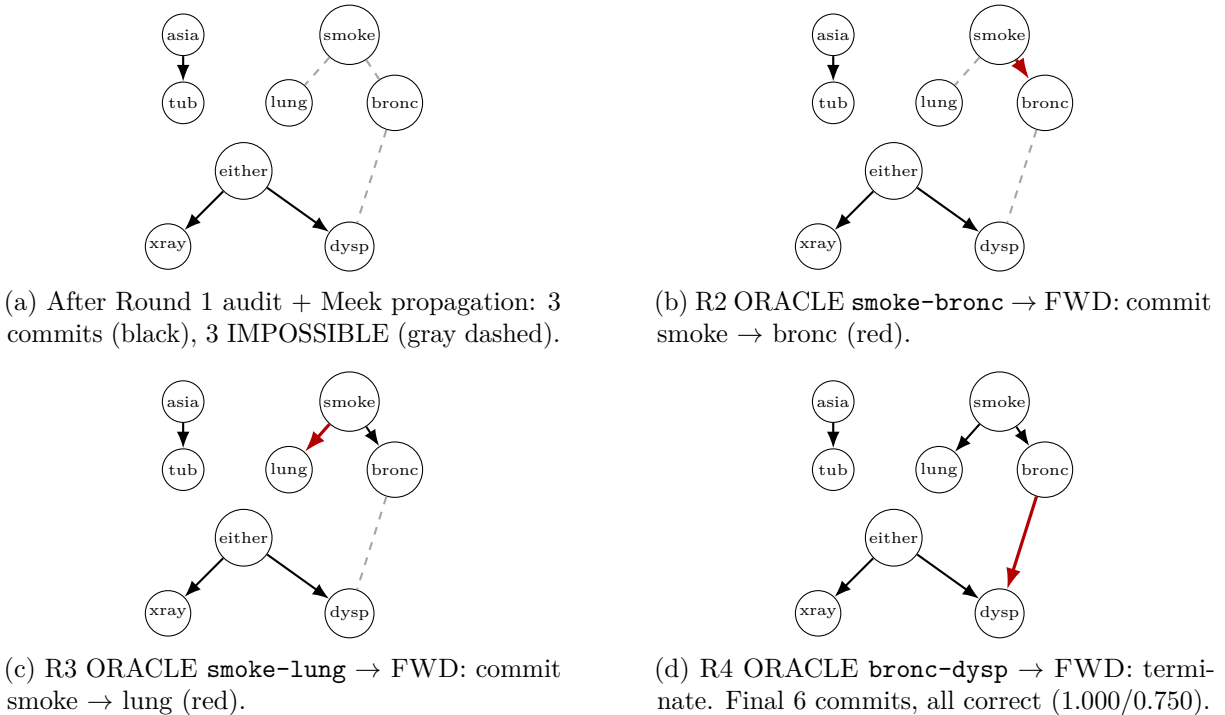


Figure 6: Iterative DAG growth on asia. Black solid arrows are committed edges; the red thick arrow in each panel marks the *newly* added edge in that round. Dashed gray edges remain IMPOSSIBLE. Round 1 auto-resolves 3 edges (cascade audit + Meek propagation) at zero prior cost; rounds 2–4 each add one directional edge from a single oracle answer. Panel (d) is the protocol’s output: 6 commits, all correct (precision 1.000, recall 0.750 = 6/8 GT edges).

The walk-through illustrates three properties of the protocol:

- **Panel (a):** the cascade’s  $L_0$  identifies two directional edges directly from data (RESOLVED\_LINEAR\_ANM); Meek-R1 propagation adds a third. Three IMPOSSIBLE edges remain.
- **Panels (b)–(d):** each oracle query asks one certificate-specific question and gets one of FWD/BWD/ABSENT. The protocol records which question is being asked, so the practitioner can audit the iteration trace and verify reproducibility.

- **Termination:** when IMPOSSIBLE is empty, the protocol emits the final DAG. Every committed edge is justified by either the data (cascade/propagation) or a specific practitioner answer to a specific question.

The second case study is the Sachs protein-signalling benchmark, which presents a denser skeleton and a more demanding cascade audit. Sachs has  $V = 11$  proteins and 20 ground-truth edges. The cascade audit produces 1 RESOLVED\_LINEAR\_ANM commit and 8 RESOLVED\_MEDIATED drops (multi-tier mediator search); the iterative loop then issues 21 targeted oracle queries. Figure 7 shows three snapshots: after audit (panel a), at the iteration midpoint (panel b), and at termination (panel c). The colour code is the same as Figure 6.

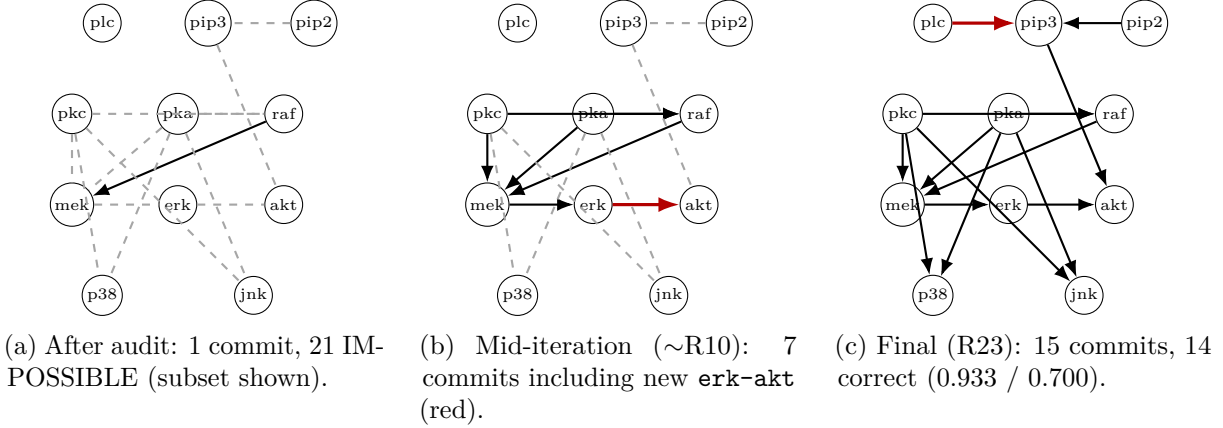


Figure 7: Sachs walk-through ( $V = 11$ ,  $N = 2000$ , propagation disabled, multi-tier mediator search enabled). Edges shown are representative of GT structure; the multi-tier mediator search drops 8 spurious skeleton edges at audit time, leaving 21 IMPOSSIBLE that get oracle-queried.

The third case study is the financial-returns benchmark **stocks\_banks**, on which the cascade defers every candidate to the oracle. **stocks\_banks** has  $V = 10$  assets and 11 ground-truth edges:  $ust10y \rightarrow xlf$ , the sector ETF  $xlf \rightarrow \{JPM, BAC, WFC, GS, MS, C, USB, PNC\}$ , and two mega-to-regional links ( $JPM \rightarrow USB$ ,  $JPM \rightarrow PNC$ ). The cascade auto-commits *zero* edges on this benchmark (all 45 skeleton candidates are IMPOSSIBLE\_LATENT\_LIKELY because daily returns are highly cross-correlated through market-beta); every edge goes to the oracle. Figure 8 shows three representative snapshots; the protocol terminates at 1.000 precision and 1.000 recall.

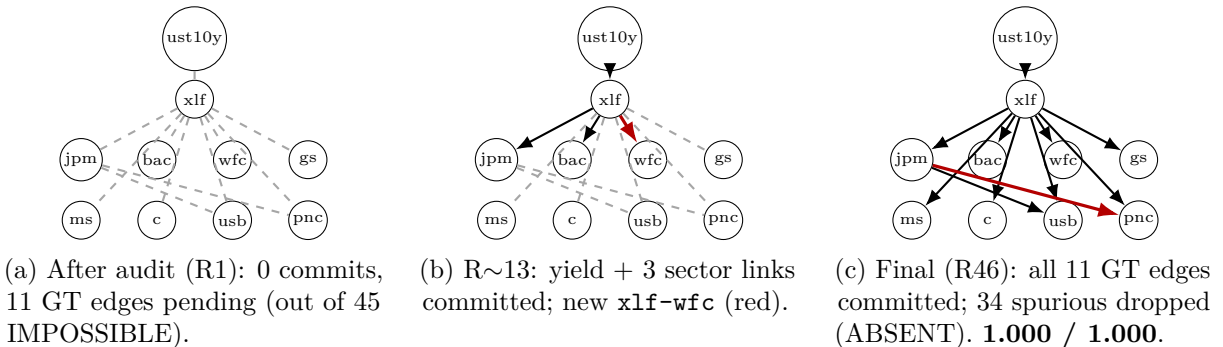


Figure 8: **stocks\_banks** walk-through. The cascade refuses to auto-commit any edge on dense market-beta-correlated data, so all 45 candidates go to the oracle. Each FWD/BWD answer adds a directional edge; each ABSENT answer drops a spurious one. Result: perfect recovery in 45 oracle queries.

The fourth case study is the child benchmark, a hub-structured clinical-reasoning network that exercises constraint propagation. The full child DAG has  $V = 20$  nodes; we show only the hub subgraph around the clinical decision pathway (BirthAsphyxia  $\rightarrow$  Disease  $\rightarrow$  {LungParench, LungFlow, CardiacMixing, HypDistrib}  $\rightarrow$  {CO<sub>2</sub>, ChestX-ray}). After cascade audit + propagation, 3 edges are auto-committed and 19 oracle queries complete the DAG at 0.955 precision and 0.840 recall.

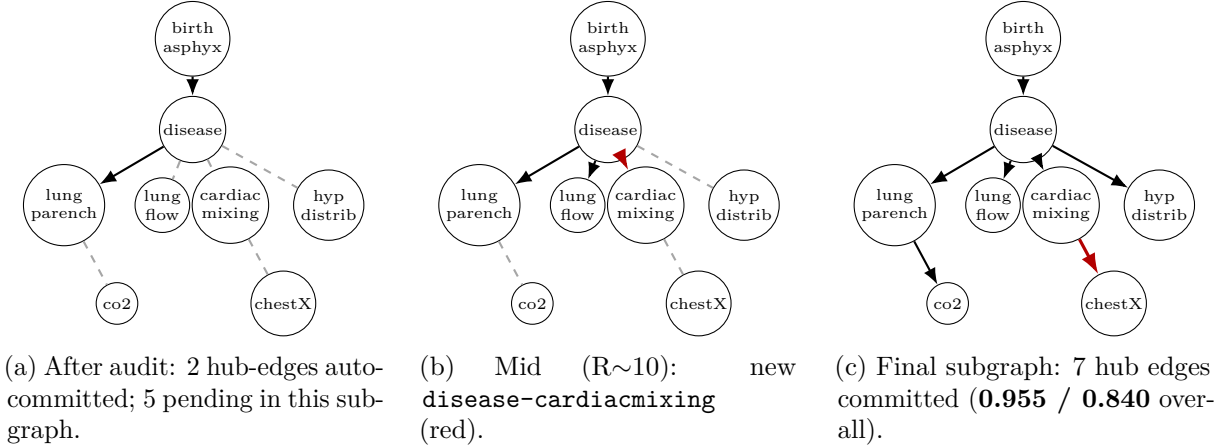


Figure 9: child walk-through, hub-node subgraph view (8 of 20 nodes shown). The hub is **disease**, with all major clinical symptoms downstream. Edges outside the hub-subgraph evolve in parallel; the full  $V = 20$  DAG is too dense for a static figure.

The final case study is alarm, the largest of the four benchmarks at  $V = 37$ . The full alarm DAG has  $V = 37$  nodes; we show the cardiovascular hub subgraph (HISTORY  $\rightarrow$  LVFAILURE  $\rightarrow$  LVEDVOLUME  $\rightarrow$  STROKEVOLUME  $\rightarrow$  CO  $\rightarrow$  BP) plus the heart-rate branch (HR  $\rightarrow$  CO). The cascade audit + Meek propagation auto-commit 2 edges, and 31 oracle queries complete the full DAG at 0.810 precision and 0.739 recall.

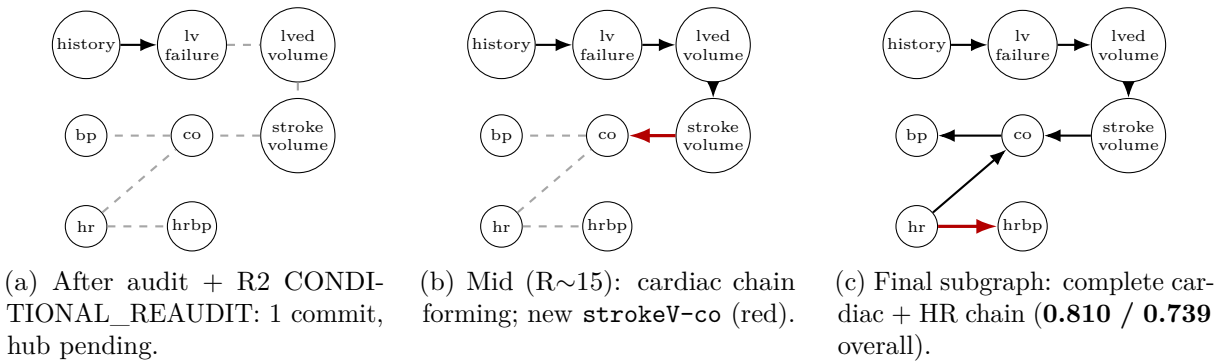


Figure 10: alarm walk-through, cardiovascular-hub subgraph view (8 of 37 nodes shown). The hub is the cardiac output chain; side branches (e.g., respiratory) evolve in parallel. The full  $V = 37$  DAG is too dense to render statically; the trace CSV records the complete 31-round event sequence.